# Manipulating the Motion of a Single Trapped Atom

C. Monroe,* D.M. Meekhof, B.E. King, D. Leibfried, W.M. Itano, and D.J. Wineland

*National Institute of Standards and Technology, Boulder, CO 80303*

## Introduction

A single atom confined in an electromagnetic trap (see Fig. 1) has many similarities to a molecule. Spectroscopy reveals both internal electronic structure and external vibrational structure. In the case of a trapped atom, the vibrational states can be controlled to a high degree, primarily because the effective vibrational potential is externally applied and can be made almost purely harmonic. By coupling the electronic and vibrational states of a trapped atom with laser radiation, motional wavepackets of the atom can be manipulated and interesting states of motion can be created which exhibit highly nonclassical behavior.

In this article, we describe experiments which control the bound states of a "molecule" formed by a single trapped atomic ion bound to a harmonic trap. We create[1] (i) Fock states (eigenstates of vibration) including the n=0 zero-point vibrational ground state, (ii) coherent states, where the wavepacket orbit corresponds most closely to classical oscillation in the trap, (iii) squeezed states, in which the wavepackets undergo a "breathing" mode in the trap, and (iv) "Schrödinger Cat" states of motion[2], where the trapped ion is placed in a coherent superposition of spatially separated coherent states. Such states of motion are useful for a number of

(1) Meekhof, D.M.; Monroe, C.; King, B.E.; Itano, W.M.; Wineland, D.J., *Phys. Rev. Lett.* **1996**, *76*, 1796.

applications, including issues involving quantum measurement theory, sensitive electronic detection[3], spectroscopy below the quantum limit[3], quantum computers[4,5], and the study of quantum decoherence[6].

**Internal and External States of a Trapped Ion**

Since $^9Be^+$ is hydrogenic, the internal energy level structure of its outer 2S electron is fairly simple. We isolate two particular hyperfine energy levels of the electron in its $2S_{1/2}$ orbital ground state. The $|F=2, m_F=2\rangle$ (denoted by $|\downarrow\rangle$) and $|F=1, m_F=1\rangle$ (denoted by $|\uparrow\rangle$) levels are separated in frequency by $\omega_{HF}/2\pi \approx 1.25$ GHz. The other $2S_{1/2}$ Zeeman levels are well resolved from these two states by the application of a ≈0.2 mT magnetic field. The electronic levels of interest are summarized in Fig. 2.[9]

In order to controllably access the vibrational levels of an atom oscillating in a trap, it is necessary that the vibrational level spacing (trap oscillation frequency) be much larger than any atomic or motional relaxation rates. To this end, we have designed a rf (Paul) ion trap [7,8,9] which strongly confines a single $^9Be^+$ ion. We realize harmonic oscillation frequencies of $(\omega_x, \omega_y, \omega_z)/2\pi$

---


(2) Monroe, C.; Meekhof, D.M.; King, B.E.; Wineland, D.J., *Science* **1996**, *272*, 1100.

(3) Heinzen, D.J.; Wineland, D.J., *Phys. Rev. A* **1990**, *42*, 2977; Wineland, D.J.; Bollinger, J.J.; Itano, W.M.; Heinzen, D.J., *Phys. Rev. A* **1994**, *50*, 67.

(4) Lloyd, S., *Scientific American*, October **1995**, *273*, 140; DiVincenzo, D.P., *Science* **1995**, *270*, 255; Bennett, C.H. *Physics Today* October **1995**, *48*, 24.

(5) Cirac, J.I.; Zoller, P. *Phys. Rev. Lett.* **1995**, *74*, 4091; Monroe, C.; Meekhof, D.M.; King, B.E.; Itano, W.M.; Wineland, D.J. *Phys. Rev. Lett.* **1995**, *75*, 4714.

(6) Zurek, W.H. *Physics Today*, October **1991**, *44*, 36.

(7) Dehmelt, H.G. *Adv. Atom. Mol. Phys.* **1967**, *3*, 53; **1969**, *5*, 109.

(8) Jefferts, S.R.; Monroe, C.; Bell, E.W.; Wineland, D.J. *Phys. Rev. A* **1995**, *51*, 3112.

(9) Monroe, C.; Meekhof, D.M.; King, B.E.; Jefferts, S.R.; Itano, W.M.; Wineland, D.J.; Gould, P. *Phys. Rev. Lett.* **1995**, *75*, 4011.

≈ (11, 19, 29) MHz of atomic motion along the three principal axes of the trap. As shown in Fig 2, the internal $^9Be^+$electronic states $|\downarrow\rangle$ and $|\uparrow\rangle$ are accompanied by the ladder of external harmonic oscillator levels of energy $E_n = \hbar\omega(n+½)$, where we have only considered the x-dimension of the oscillator ($\omega \equiv \omega_x$) and its associated quantum number $n \equiv n_x \varepsilon (0,1,2,...)$.

Coherent manipulation of the state of motion is accomplished by applying a pair of laser beams (R1 and R2) to the trapped ion (Fig 2a). By tuning the difference frequency of R1 and R2 to be near $\omega_{HF}$, two-photon stimulated Raman transitions between the $2S_{1/2}$ electronic ground states can be driven. In general, this Raman process alters both the internal electronic state of the ion *and* the vibrational state of the ion in the trap. The two Raman beams are generated from a single laser source and modulator, allowing excellent stability of their relative frequency and phase. Both beams are near $\lambda \approx 313$ nm and detuned $\Delta \approx 10$ GHz from an excited $2P_{1/2}$ electronic orbital state (radiative linewidth $\gamma/2\pi \approx 19.4$ MHz). Because $\Delta >> \gamma$, the excited $2P_{1/2}$ state can be adiabatically eliminated, resulting in a stimulated Raman coupling between the two 2S ground states ($|\downarrow\rangle$ and $|\uparrow\rangle$) exhibiting a linewidth inversely proportional to the interaction time. When R1 and R2 are applied to the ion with wavevector difference $\delta\mathbf{k} = \mathbf{k_1}-\mathbf{k_2}$ along the x-direction, the

$$\hbar_{eff} = g\left(\sigma_+ e^{i\eta(a^-+a)-i\delta t} + \sigma_- e^{-i\eta(a^-+a)+i\delta t}\right) .$$

effective coupling Hamiltonian in the rotating-wave approximation is given by[1]:

In this expression, $\sigma_\pm$ is the raising (lowering) operator of the internal states $|\downarrow\rangle$ and $|\uparrow\rangle$, and $a^\dagger$ and a are the creation and annihilation operators for the state of harmonic vibration: $a|n\rangle = n^{1/2}|n\text{-}1\rangle$ and $a^\dagger|n\rangle = (n+1)^{1/2}|n+1\rangle$. The parameter g is the coupling strength which depends on

$\Delta$ and the intensity of the laser beams,[9] $\eta = |\delta\mathbf{k}|x_0$ is the Lamb-Dicke parameter ($x_0 = (\hbar/2m\omega)^{1/2}$ $\approx$ 7 nm is the spatial spread of the n=0 ground vibrational state), and $\delta$ is the relative frequency of the two Raman beams R1 and R2 with respect to the free atom resonance. The Lamb-Dicke parameter controls the amount of coupling between the internal electronic states and the external vibrational states, and has the value $\eta \approx 0.2$ in the experiment[9]. By setting $\delta\mathbf{k}$ to be parallel to the x-axis of the trap, there is almost no coupling between the 2LS and motion in the y and z directions.

By tuning the relative frequency to $\delta = \omega(n'-n)$, Raman transitions are driven between the levels $|\downarrow,n\rangle$ and $|\uparrow,n'\rangle$. In this case, $H_{eff}$ is dominated by a single stationary term, resulting in the

$$\langle\uparrow,n'|\hbar_{eff}|\downarrow,n\rangle = g\langle\uparrow,n'|\sigma_+ e^{i\eta(a^\dagger+a)} + \sigma_- e^{-i\eta(a^\dagger+a)}|\downarrow,n\rangle .$$

coupling matrix element:

This coupling describes a coherent Rabi flopping process between the states $|\downarrow,n\rangle$ and $|\uparrow,n'\rangle$ induced by the laser beams. In the Lamb-Dicke limit, where $\eta\langle a^\dagger+a\rangle \ll 1$, the above matrix

$$\Omega_{n,n'} \approx g\left(\frac{\eta^{|n'-n|}}{|n'-n|!}\right)$$

element can be expanded to its lowest order, resulting in a Rabi flopping frequency of

where $|n'-n|$ is the sideband order, and $n_>$ ($n_<$) is the greater (lesser) of n and n′. The exact Rabi frequency includes terms of higher order in the Lamb-Dicke parameter $\eta$, which only become

significant for larger values of n.[1,10] These couplings between different states of vibration are similar to the Franck-Condon factors in molecular spectroscopy, where the "molecule" in this case is the ion harmonically bound to the apparatus. A Rabi "π-pulse" from $|\downarrow\rangle|n\rangle \rightarrow |\uparrow\rangle|n'\rangle$ corresponds to applying the Raman beams for a duration $\tau$ such that $\Omega_{n,n'}\tau = \pi/2$.

We will be primarily interested in three types of transitions: the "carrier" (n′-n = 0), the "first red sideband" (n′ - n = -1), and the "first blue sideband" (n′ - n = +1). These transitions are selected by setting the tuning $\delta$ of the Raman beams and the duration of the applied pulses. The carrier ($\delta = 0$) drives transitions between states $|\downarrow,n\rangle \rightarrow |\uparrow,n\rangle$ with Rabi frequency $\Omega_{n,n} = g$. The first red sideband ($\delta = -\omega$) drives transitions between states $|\downarrow,n\rangle \rightarrow |\uparrow,n-1\rangle$ with Rabi frequency $\Omega_{n,n-1} = g\sqrt{n}$ and is analogous to anti-Stokes vibrational Raman scattering in molecular spectroscopy. The first blue sideband ($\delta = +\omega$), drives transitions between states $|\downarrow,n\rangle \rightarrow |\uparrow,n+1\rangle$ with Rabi frequency $\Omega_{n,n+1} = g(n+1)^{1/2}$ and is analogous to Stokes Raman scattering.

The internal state ($|\downarrow\rangle$ or $|\uparrow\rangle$) of the trapped ion is detected by applying near-resonant $\sigma^+$-polarized laser radiation (beam D2, Fig. 2b) between the $|\downarrow\rangle$ and $^2P_{3/2}(F=3, m_F=3)$ energy levels. Because this is a cycling transition, millions of photons are scattered from the ion if and only if the ion is in the $|\downarrow\rangle$ state, regardless of the vibrational state. The fluorescence is recorded, resulting in almost unit detection efficiency of the ion's internal state.[9]

Following the creation of a particular motional state in the $|\downarrow\rangle$ internal level, we detect the motional state as follows: A Raman "probe" pulse is applied for a time $\tau$ and the probability $P_\downarrow(\tau)$ that the ion in the $|\downarrow\rangle$ internal state is measured. The experiment is repeated (state

(10) Wineland, D.J.; Itano, W.M.; *Phys. Rev. A* **1979**, *20*, 1521; Vogel, W.; de Matos Filho,

creation, Raman probe pulse, detection of $|\downarrow\rangle$), while slowly stepping the interaction time $\tau$.

$$P_{\downarrow}(\tau) = \sum_{n=0}^{\infty} P_n \cos^2(g\sqrt{n+1}\tau)$$

When the Raman probe pulse is tuned to the blue sideband, the expected signal is

where $P_n$ is the probability distribution of vibration state n. This time-domain signal is a record of Rabi flopping among all populated vibrational states. Since the blue sideband Rabi frequencies $\Omega_{n,n+1} \approx g(n+1)^{1/2}$ depend on n, the measured signal $P_{\downarrow}(\tau)$ can be inverted (Fourier cosine transform) allowing the probability distribution of vibrational states $P_n$ to be extracted.

**Sideband Laser Cooling to the n=0 Zero-Point Energy and Higher Fock States of Vibration**

By tuning near-resonant laser beams slightly red of the $2S_{1/2} \rightarrow 2P_{3/2}$ resonance (Fig 2b), the ion is Doppler cooled so that the vibrational quantum number follows a thermal distribution with $\langle n \rangle \approx 1$.[11] In order to coherently manipulate the state of motion and remove thermal fluctuations, we desire to cool the ion further, to the n=0 ground state. We achieve this by employing resolved-sideband laser-cooling[9,11] with the narrow 2-photon stimulated Raman transitions discussed above. The Raman beams are tuned to the first red-sideband (anti-Stokes line) and applied for a duration which results in a $\pi$-pulse ($|\downarrow\rangle|n\rangle \rightarrow |\uparrow\rangle|n\text{-}1\rangle$). Next, laser pulses resonantly recycle the internal state by coupling the $|\uparrow\rangle|n\text{-}1\rangle$ state to the 2P excited state resulting in spontaneous emission to the $|\downarrow\rangle|n\text{-}1\rangle$ state with high probability (beam D1 of Fig

---

R.L. *Phys. Rev. A* **1995**, *52*, 4214.

(11) Wineland, D.J.; Itano, W.M. *Physics Today* **1987**, *40*, No. 6, 34.

2b). By repeating this cycle (red sideband π-pulse + resonant recycle) many times, we are able to cool the ion to the $|\downarrow\rangle|n=0\rangle$ vibrational ground state with a probability in excess of 0.95.[9] This is verified by measuring the almost complete depletion of the red sideband (anti-Stokes) line intensity. To a good approximation, this results in a minimum-uncertainty wavepacket of size $x_0$ at the bottom of the trap.

A Fock state is simply a motional state of a particular vibrational quantum number n, or an energy eigenstate of motion. From the vibrational ground state, we generate higher Fock states by applying several π-pulses of the Raman beams. For instance, we create the $|\downarrow\rangle|n=2\rangle$ Fock state from an initial $|\downarrow\rangle|n=0\rangle$ state by applying a π-pulse on the blue sideband followed by a π-pulse on the red sideband, so that the ion steps through the states $|\downarrow\rangle|0\rangle \rightarrow |\uparrow\rangle|1\rangle \rightarrow |\downarrow\rangle|2\rangle$. Since the probability distribution for Fock state n is concentrated on just one vibrational energy level, the expected signal (Eq. 4) is a simple sinusoid: $P_\downarrow(\tau) = \cos^2[g\tau(n+1)^{1/2}]$. In Fig. 3, the measured flopping signal $P_\downarrow(\tau)$ is shown for the initial $|n=0\rangle$ Fock state as well as the $|n=4\rangle$ Fock state. The Rabi oscillations of the n=4 Fock state are faster by the expected factor of $\approx\sqrt{5}$. We have produced and detected Fock states as high as $n\approx16$.

**Coherent States and Squeezed States**

A coherent state of motion $|\alpha\rangle$ of the ion corresponds to a displaced zero-point wave-packet oscillating in the potential well with amplitude $2\alpha x_0$. The distribution among Fock states is Poissonian: $P_n = e^{-\langle n\rangle}\langle n\rangle^n/n!$, where $\langle n\rangle = |\alpha|^2$ is the average number of vibrational quanta. As predicted in Eq. (4), the measured flopping signal for a coherent state will undergo

quantum collapses and revivals[12]. These revivals are a purely quantum effect due to the discrete energy levels and the narrow distribution of states.

Coherent states of ion motion can be produced from the $|\downarrow\rangle|0\rangle$ state by applying a resonant classical driving field[13], a "moving standing wave" of laser radiation which resonantly drives the ion via the dipole force[1], by pairs of standing waves[14], or by a sudden shift of the trap center[3]. We have used the first two methods; for the data presented here we use the first. For the classical drive, we apply a sinusoidally varying potential at the trap oscillation frequency on one of the trap compensation electrodes[8] for a fixed time (typically 10 μs) In Fig. 4a, we present a measurement of $P_{\downarrow}(\tau)$ after creation of a coherent state of motion, exhibiting the expected collapse and revival signature. This data is fitted to Eq. 4 assuming a Poissonian distribution of $P_n$, allowing only $\langle n\rangle$ to vary. All other parameters are measured from a separate trace similar to Fig. 3. The inset shows the probabilities of the Fock components, extracted by applying a Fourier cosine transform to $P_{\downarrow}(\tau)$ at the known frequencies as described above. These amplitudes display the expected Poissonian distribution of vibrational level population.

A coherent state has a definite phase relationship between the Fock state components, which is not contained in the signal $P_{\downarrow}(\tau)$. We use two methods to demonstrate the coherence of the vibrational states. First, we reverse the coherent state (by applying the same classical driving force 180° out of phase with the original force) and verify that the vibrational state returns to the $|n=0\rangle$ ground state. Secondly, we tomographically measure the complete density matrix of

(12) Eberly, J.H.; Narozhny, N.B.; Sanchez-Mondragon, J.J. *Phys. Rev. Lett.* **1980**, *44*, 1323.
(13) Carruthers, P.; Nieto, M.M. *Amer. Jour. Phys.* **1965**, *7*, 537.
(14) Cirac, J.I.; Parkins, A.S.; Blatt, R.; Zoller, P. *Phys. Rev. Lett.* **1993**, *70*, 556.

motion, including the off-diagonal coherences.[15] Both methods show the expected phase relationship between the vibrational levels.

A squeezed state of motion corresponds to a minimum uncertainty wavepacket that "breathes" in the harmonic potential. At certain times during the breathing motion, the uncertainty in position is less than the zero-point spread $x_0$.[16] A "vacuum squeezed state" of motion can be created by a parametric drive[3], by a combination of standing- and traveling-wave laser fields[14], or by a non-adiabatic drop in the trap spring constant.[3] Here we irradiate the $|n=0\rangle$ ion with two Raman beams which differ in frequency by $2\omega$, driving purely vibrational Raman transitions between the even vibrational levels without affecting the electronic state. The interaction can also be thought of as a classical parametric drive induced by an optical dipole force modulated at $2\omega$. The squeeze parameter $\beta$ (defined as the factor by which the variance of the squeezed quadrature is decreased) grows exponentially with the driving time.

The flopping data for a squeezed state is shown in Fig 4b. This data was fit to the expected population distribution for a squeezed state, allowing only the squeezing parameter $\beta$ to vary, indicating $\beta \approx 40$, corresponding to $\langle n \rangle \approx 7.1$. A squeezed vacuum state with $\beta = 40$ has 16% of its population in states above n=20. Discrimination between the various Rabi frequency $\Omega_{n,n+1}$ in these high-lying vibrational levels is small, and with the inclusion of nonlinear effects[1,10], the Rabi frequencies begin to decrease with n beyond $n \approx 20$. Because these levels can no longer be distinguished, the Fourier-cosine transform technique cannot be used to extract the level

(15) Leibfried, D.; Meekhof, D.M.; King, B.E.; Monroe, C.; Itano, W.M.; Wineland, D.J. *Phys. Rev. Lett.* **1996** (accepted for publication).

(16) Caves, C.M.; Thorne, K.S.; Drever, R.W.P.; Sandberg, V.D.; Zimmermann, M. *Rev. Mod. Phys.* **1980**, *52*, 341.

populations.

**Schrödinger Cat States**

A "Schrödinger Cat" state is known as a superposition of classical-like states. In Schrödinger's original thought experiment[17], he describes how one could in principle transform a superposition inside an atom to a large-scale superposition of a live and dead cat. In our experiment[2], we construct an analogous state at the single atom level. A superposition of internal states ($|\downarrow\rangle$ and $|\uparrow\rangle$) is transformed into a superposition of coherent motional states with different phases. The coherent states of the superposition are separated in space by mesoscopic distances much greater than the size of the atom.

This situation is interesting from the point of view of the quantum measurement problem associated with "wavefunction collapse," historically debated by Einstein and Bohr, among others[18]. One practical approach toward resolving this controversy is the introduction of quantum decoherence, or the environmentally-induced reduction of quantum superpositions into statistical mixtures and classical behavior[6]. Decoherence is commonly interpreted as a way of quantifying the elusive boundary between classical and quantum worlds, and almost always precludes the existence of macroscopic Schrödinger cat states, except at extremely short time scales[6]. The creation of mesoscopic Schrödinger cat states may allow controlled studies of quantum decoherence and the quantum/classical boundary. We note that quantum decoherence has received much interest lately due to its importance in proposals for quantum computation[4,5] and

(17) Schrödinger, E. *Naturwissenschaften* **1935**, *23*, 807.
(18) Wheeler, J.A.; Zurek, W.H. eds., *Quantum Theory and Measurement*; Princeton Univ.

quantum cryptography[4].

In the present work, we create a Schrödinger cat state of the harmonic oscillator by forming a superposition of two coherent state wavepackets of the single trapped atom with a sequence of laser pulses. Each wavepacket is correlated with a particular internal state of the atom. To analyze this state we apply an additional laser pulse to couple the internal states and we measure the resulting interference of the distinct wavepackets. The key features of our approach are that (i) we control the harmonic motion of the trapped atom to a high degree by exciting the motion from initial zero-point wavepackets to coherent state wavepackets of well-defined amplitude and phase, and (ii) wavepacket dispersion of the atomic motion is negligible.

In this experiment, the coherent states are excited with the use of a pair of Raman laser beams ("displacement beams") similar to the Raman beams used in the above experiments, except with the difference frequency of the beams matching the trap frequency. This resonantly drives the motion of the atom. The key to this experiment is that the displacement beams are both polarized $\sigma^+$, so that they do not affect the $|\downarrow\rangle$ internal state. It is this selection that allows a superposition of internal states to be transformed into a superposition of motional states.

Following laser cooling to the $|\downarrow\rangle|n=0\rangle$ as described above, we create the Schrödinger Cat state by applying several sequential pulses of the Raman beams (the evolving state of the system is summarized in Fig. 5: (1) A $\pi/2$-pulse on the carrier splits the wave-function into an equal superposition of states $|\downarrow\rangle|0\rangle$ and $|\uparrow\rangle|0\rangle$. (2) The displacement beams excite the motion correlated with the $|\uparrow\rangle$ component to a coherent state $|\alpha e^{-i\phi/2}\rangle$. (3) A $\pi$-pulse on the carrier swaps the internal states of the superposition. (4) The displacement beams excite the motion

---

Press: Princeton, NJ, 1983.

correlated with the $|\uparrow\rangle$ component to a second coherent state $|\alpha e^{i\phi/2}\rangle$. (5) A final $\pi/2$-pulse on the carrier combines the two coherent states. The relative phases ($\phi$ and the phases of steps 1,3, and 5) of the above steps are determined by the phases of the rf difference frequencies of the Raman beams, which are easily controlled by phase-locking the rf sources.

The state created after step 4 is a superposition of two independent coherent states each correlated with an internal state of the ion, in the spirit of Schrödinger's original thought experiment. We verify this superposition by recombining the coherent wavepackets in the final step 5. This results in an interference of the two wavepackets as the relative phase of the displacement forces (steps 2 and 4) is varied. The nature of the interference depends on the phases of steps (1), (3), and (5), and is set here to cause destructive interference of the wavepackets in the $|\downarrow\rangle$ state. We directly measure this interference by detecting the probability $P_\downarrow(\phi)$ that the ion is in the $|\downarrow\rangle$ internal state for a given value of $\phi$. We continuously repeat the experiment - cooling, state preparation, detection - while slowly sweeping the relative coherent state motional phase $\phi$.

In Fig. 6, we display the measured $P_\downarrow(\phi)$ for a few different values of the coherent state amplitude $\alpha$, which is set by changing the duration $\tau$ of application of the displacement beams (steps 2 and 4 from above). The presence of the interference feature near $\phi=0$ verifies that we are producing superposition states instead of statistical mixtures, and the feature clearly narrows as $\alpha$ is increased.

We extract the amplitude of the Schrödinger cat state by fitting the interference data to the expected form of the interference fringe. The extracted values of $\alpha$ agree with an independent calibration of the displacement forces. We measure coherent state amplitudes as high as

$\alpha \approx 2.97(6)$, corresponding to an average of $\langle n \rangle \approx 9$ vibrational quanta in the state of motion. This indicates a maximum spatial separation of $4\alpha x_0 = 83(3)$ nm, which is significantly larger than the single wavepacket size of $x_0 = 7.1(1)$ nm as well as a typical atomic dimension ($\approx$0.1 nm). The individual wavepackets are thus clearly separated in phase space.

Of particular interest is the fact that as the separation of the cat state is made larger, the decay from superposition to statistical mixture (decoherence) becomes faster. In the experiment, decoherence is expected to result in the loss of visibility in the interference pattern. In Fig. 6d, the observed loss of contrast at the largest observed separation may already indicate the onset of decoherence. The precise control of quantum wavepackets in this version of "Schrödinger's cat" provides a very sensitive indicator of quantum decoherence, whose characterization is of great interest to quantum measurement theory[18] and applications such as quantum computing.[4,5]

We have demonstrated how the quantum wavepackets of a single harmonically bound atom can be controlled to a high degree, allowing the preparation of Fock, coherent, squeezed, and "Schrödinger cat" states of motion. The experiments are complementary to recent results in molecular vibrational wavepacket control,[19] except that the effective "molecule" in this case is formed by the binding between an atom and an external electromagnetic trap. Future experiments in this system may lead to the coherent control of the vibrational modes of a crystal of trapped ions (see Fig. 1), and the investigation of quantum systems at the mesoscopic scale.

(19) B. Kohler, et al., *Acc. Chem. Res.* **1995**, 28, 133.

We acknowledge support from the U.S. National Security Agency, Office for Naval Research, and the Army Research office.

## FIGURE CAPTIONS

**Figure 1.** Image of one, two, and three beryllium ($^9Be^+$) ions held in a rf (Paul) electromagnetic trap. The ions are illuminated by resonant laser light and the scattered fluorescence is collected. The resolution (a few micrometers) is limited by the optical imaging system and is much larger than the actual size of the atomic wavepackets (a few nanometers). All of the experiments reported here deal with a single trapped ion.

**Figure 2.** (a) Electronic (internal) and motional (external) energy levels (not to scale) of the trapped $^9Be^+$ ion, coupled by indicated laser beams R1 and R2. The difference frequency of the Raman beams R1 and R2 is set near $\omega_{HF}/2\pi \approx 1.250$ GHz, providing a two-photon Raman coupling between the $2S_{1/2}(F=2, m_F=2)$ and $2S_{1/2}(F=1, m_F=1)$ hyperfine ground states (denoted by $|\downarrow\rangle$ and $|\uparrow\rangle$ respectively). The motional energy levels are depicted by a ladder of vibrational states separated in frequency by the trap frequency $\omega_x$. The Raman beams are detuned $\Delta \approx -12$ GHz from the $2P_{1/2}(F=2, m_F=2)$ excited state. As shown, the Raman beams are tuned to the red sideband. (b) Detection of the internal state is accomplished by illuminating the ion with $\sigma^+$-polarized "detection" beam D2, which drives the cycling $^2S_{1/2}(F=2, m_F=2) \rightarrow 2P_{3/2}(F=3, m_F=3)$ transition, and observing the scattered fluorescence. The vibrational structure is omitted from the figure since it is not quite resolved (2P radiative linewidth $\gamma/2\pi \approx 19.4$ MHz). Beam D1, also $\sigma^+$ polarized, allows the spontaneous recycling from the $|\uparrow\rangle$ to $|\downarrow\rangle$ state.

**Figure 3.** (a) $P_\downarrow(\tau)$ for an initial $|\downarrow\rangle|n=0\rangle$ Fock state driven with a Raman probe tuned to the first blue sideband (Stokes transition). (b) Same as (a) for the case of an initial $|\downarrow\rangle|n=4\rangle$ Fock state. Note the rates of Rabi oscillations scale approximately as $(n+1)^{1/2}$ or $\sqrt{5}$. The solid curves

are fits to an exponentially decaying sinusoid. Each data point in represents an average of ≈4000 measurements, or 1 s of integration.

**Figure 4.** (a) $P_{\downarrow}(\tau)$ for a coherent state driven with a Raman probe tuned to the blue sideband (Stokes transition), showing collapse and revival behavior. The solid curve is a single-parameter fit to a coherent state distribution, yielding $\langle n \rangle = 3.1(1)$. The inset shows the results of inverting the time-domain data by employing a Fourier cosine transform at the known Rabi frequencies $\Omega_{n,n+1}$, fitted to a Poissonian distribution, yielding $\langle n \rangle = 2.9(1)$. (b) $P_{\downarrow}(\tau)$ for a squeezed state driven by the blue sideband interaction, showing a complicated behavior involving many vibrational levels. The solid curve is a single-parameter fit to a squeezed state distribution, yielding a squeeze parameter $\beta = 40(10)$. Each data point in both traces represents an average of ≈4000 measurements, or 1 s of integration.

**Figure 5.** Evolution of the idealized position-space atomic wavepacket entangled with the internal states $|\downarrow\rangle$ and $|\uparrow\rangle$ during creation of a Schrödinger cat state with $\alpha=3$ and $\phi=\pi$ (displacement forces in opposite directions). The wavepackets are snapshots in time, taken when the atom is at the extrema of motion in the harmonic trap (represented by the parabolas). The area of the wavepackets corresponds to the probability of finding the atom in the given internal state. (a) The initial wavepacket corresponds to the quantum ground state of motion following laser-cooling. (b) The wavepacket is split following a $\pi/2$-pulse on the carrier. (c) The $|\uparrow\rangle$ wavepacket is excited to a coherent state by the force $\mathbf{F_1}$ of the displacement beams. Note the force acts only on the $|\uparrow\rangle$ wavepacket, thereby entangling the internal and motional systems. (d) The $|\downarrow\rangle$ and $|\uparrow\rangle$ wavepackets are exchanged following a $\pi$-pulse on the carrier. (e) The $|\uparrow\rangle$ wavepacket is excited to a coherent state by the displacement beam force $\mathbf{F_2}$, which in general has

a different phase with respect to the force in (c) ($\mathbf{F_2} = -\mathbf{F_1}$ in the figure). The state shown in (e) is analogous to a Schrödinger cat state. (f) The $|\downarrow\rangle$ and $|\uparrow\rangle$ wavepackets are finally combined following a $\pi/2$-pulse on the carrier.

**Figure 6.** Measured and fit interference signal $P_\downarrow(\phi)$ versus the phase difference $\phi$ of two coherent states. Curves (a) to (d) represent measurements for various separations of the coherent states. As they get further apart, the destructive interference feature near $\phi=0$ narrows. The lines are fits of the interference pattern to theory, yielding the values of $\alpha$ indicated. The fit in curve (d) includes a loss of contrast and represents a superposition of two $x_0 \approx 7$ nm wavepackets with a maximum separation of $4\alpha x_0 \approx 80$ nm. Curve (e) is a theoretical plot for a pair of coherent states with $\alpha=6$. Each data point in (a) to (d) represents an average of ≈4000 measurements, or 1 s of integration.

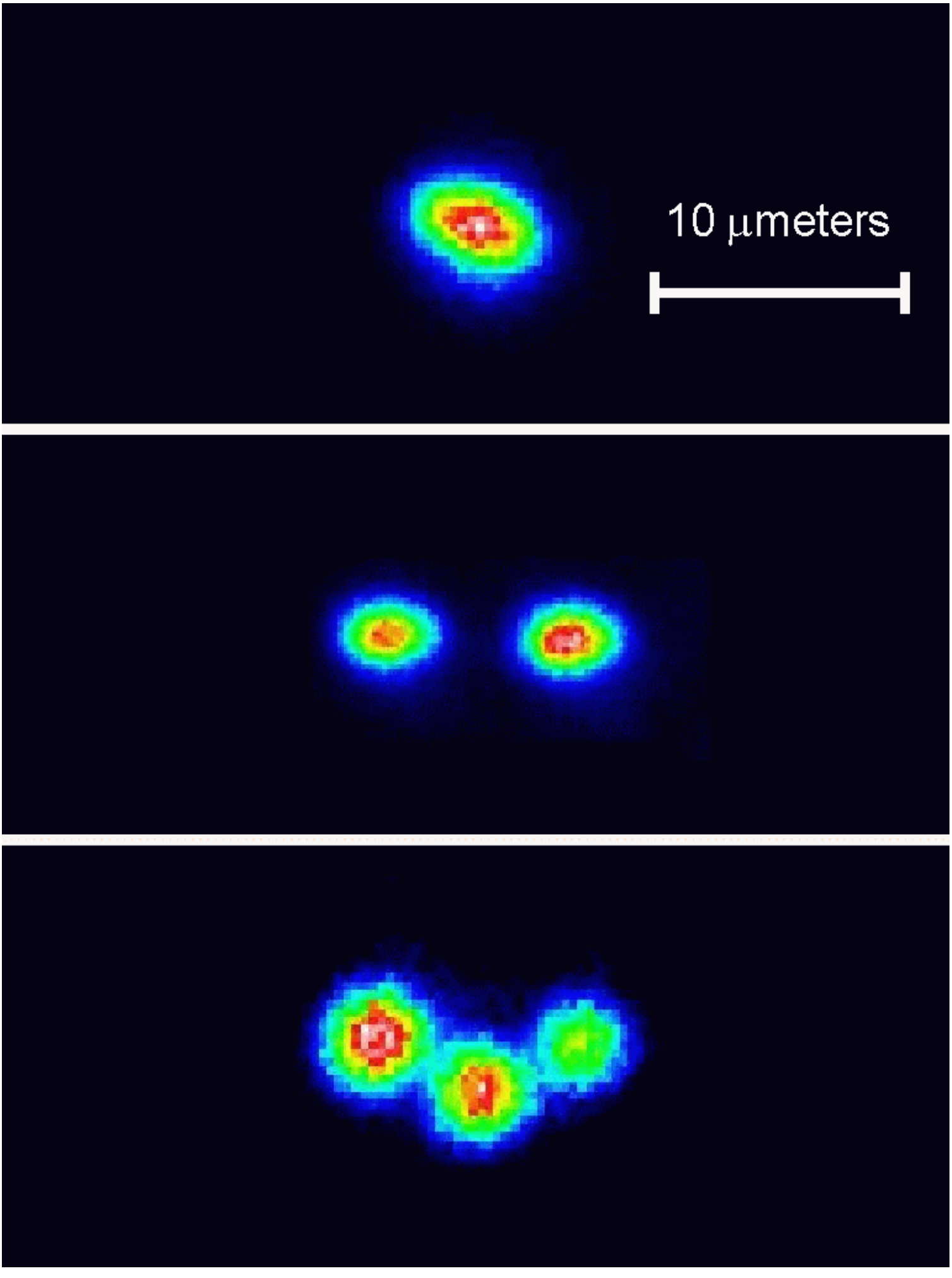
10 μmeters

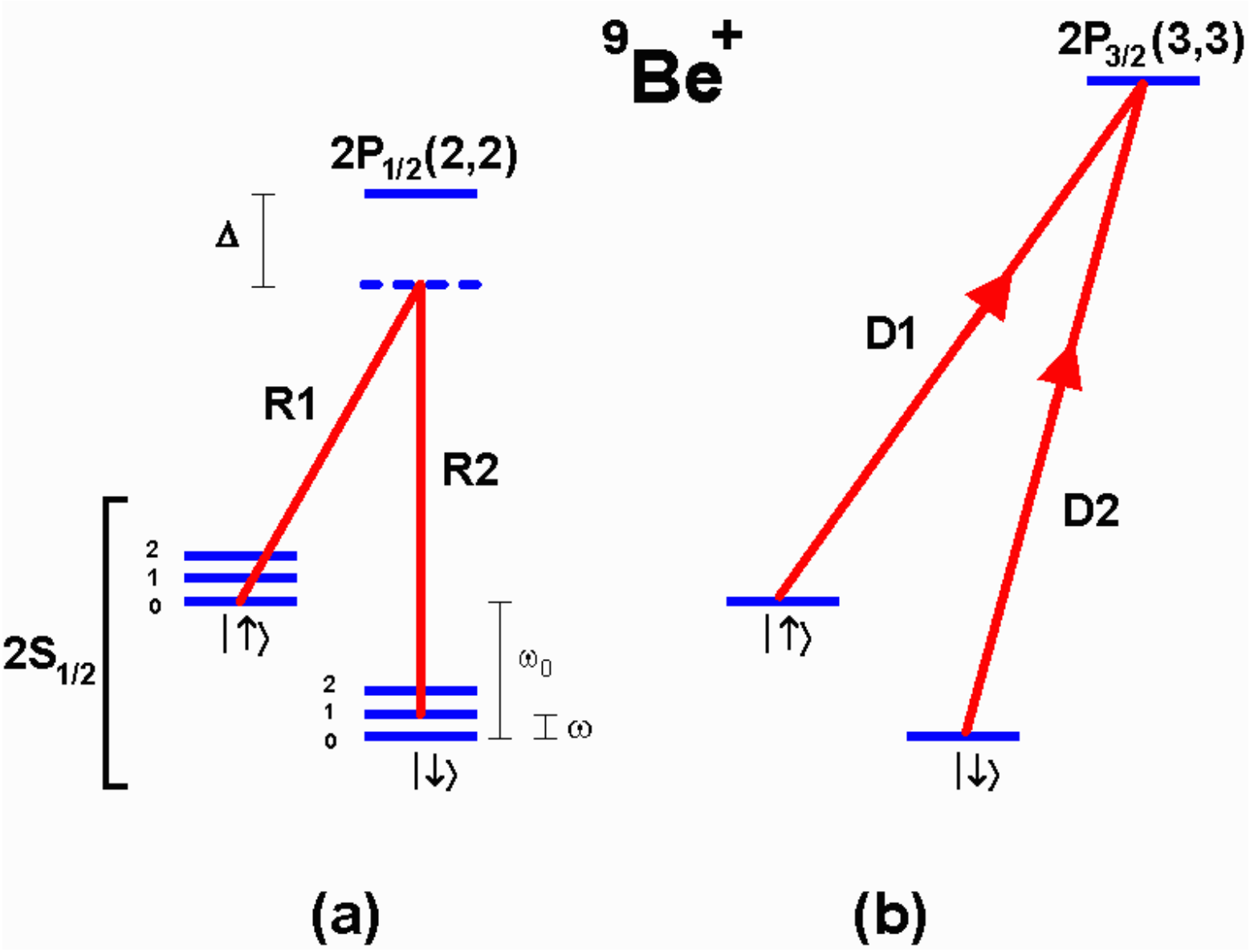
$^9Be^+$
$2P_{1/2}(2,2)$
Δ
R1
R2
2
1
0
$2S_{1/2}$
$|\uparrow\rangle$
$\omega_0$
ω
$|\downarrow\rangle$
(a)
$2P_{3/2}(3,3)$
D1
D2
$|\uparrow\rangle$
$|\downarrow\rangle$
(b)

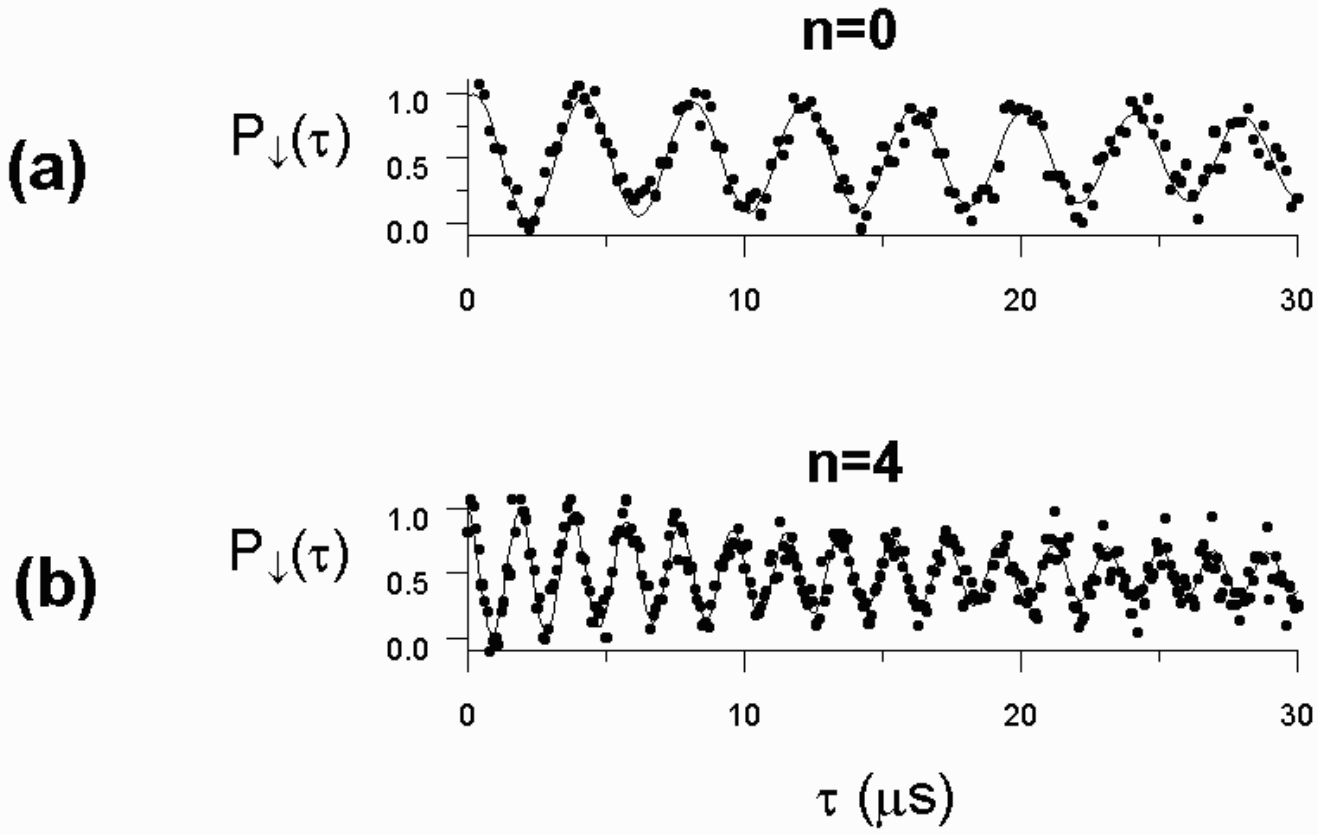
(a)
n=0
$P_{\downarrow}(\tau)$
1.0
0.5
0.0
0
10
20
30
(b)
n=4
$P_{\downarrow}(\tau)$
1.0
0.5
0.0
0
10
20
30
τ (μs)

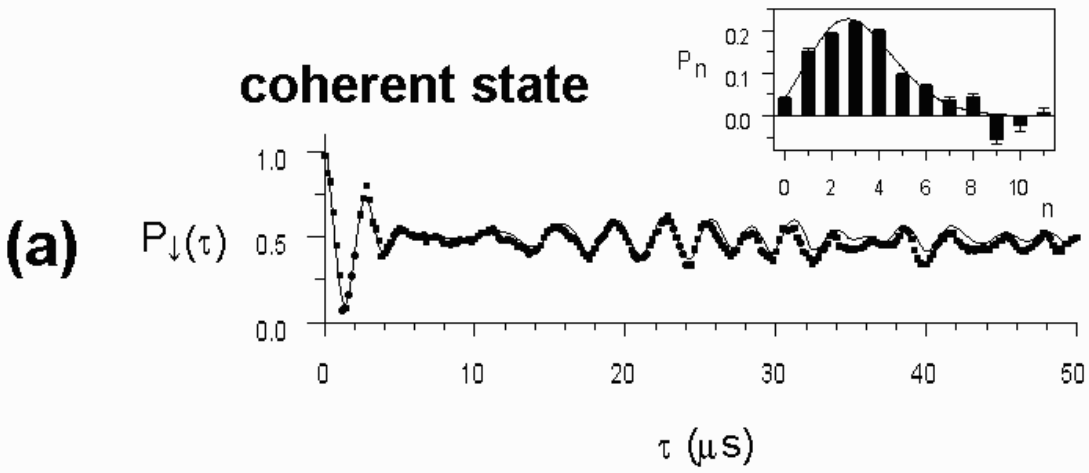
(a)
coherent state
$P_\downarrow(\tau)$
1.0
0.5
0.0
0
10
20
30
40
50
$\tau$ ($\mu$s)
$P_n$
0.2
0.1
0.0
0
2
4
6
8
10
n

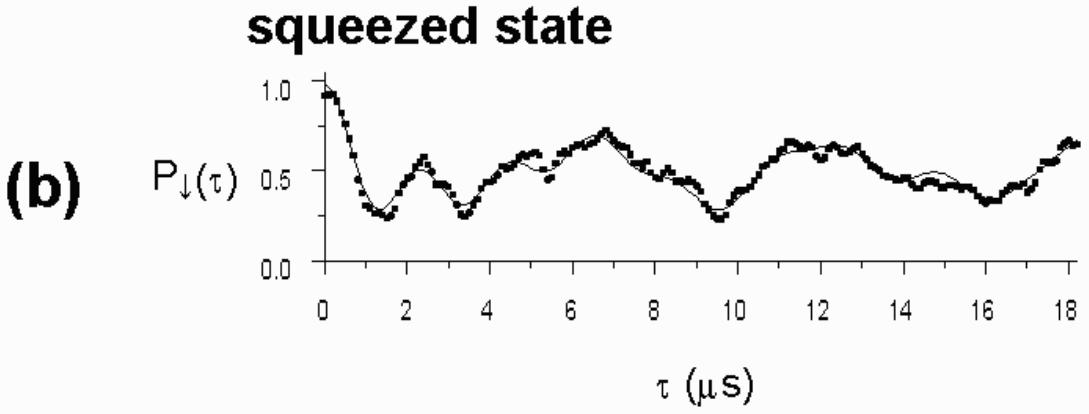
(b)
squeezed state
$P_\downarrow(\tau)$
1.0
0.5
0.0
0
2
4
6
8
10
12
14
16
18
$\tau$ ($\mu$s)

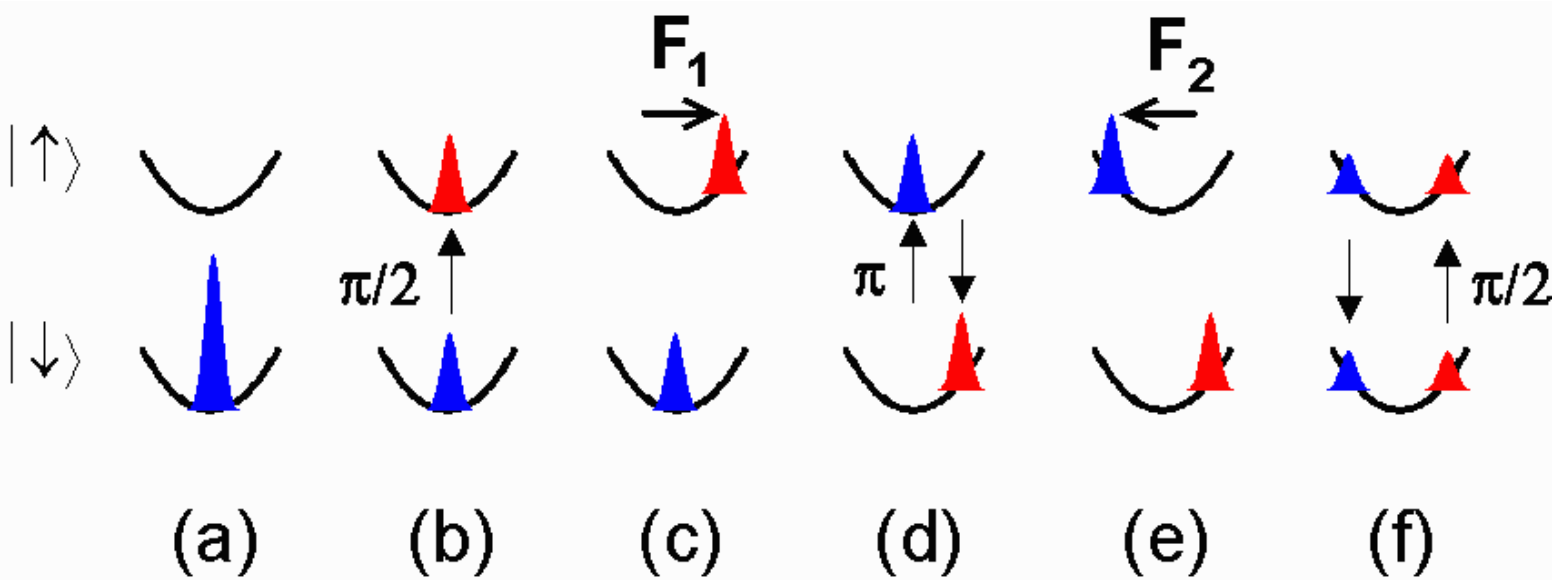
F1
F2
|↑⟩
|↓⟩
π/2
π
π/2
(a)
(b)
(c)
(d)
(e)
(f)

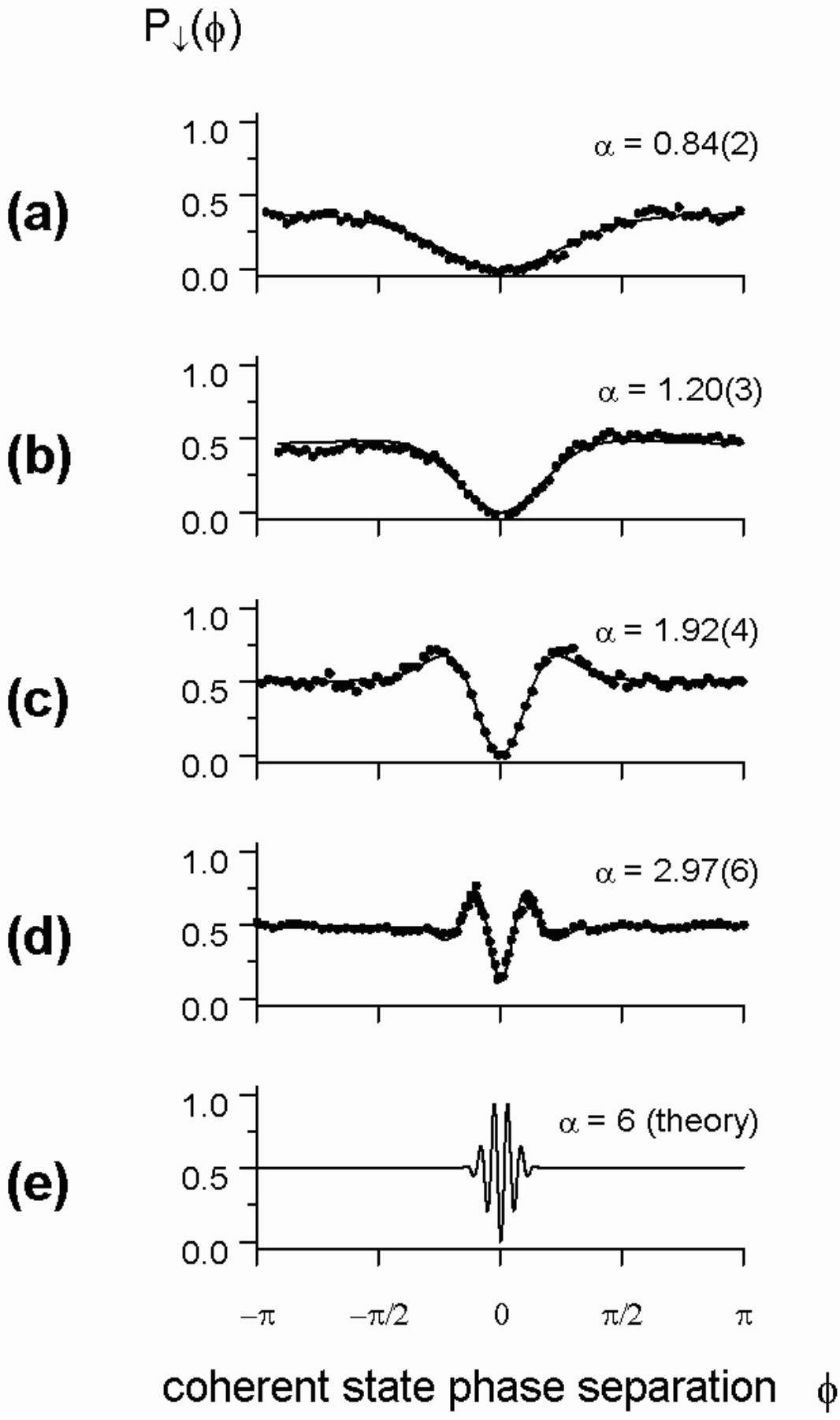
$P_{\downarrow}(\phi)$
(a)
(b)
(c)
(d)
(e)
1.0
0.5
0.0
α = 0.84(2)
α = 1.20(3)
α = 1.92(4)
α = 2.97(6)
α = 6 (theory)
−π
−π/2
0
π/2
π
coherent state phase separation φ